Journal of Traditional Chinese Medicine

ISSN 2709-7240 | Volume 3

Case Report Open Access

Therapeutic Efficacy and Molecular Mechanisms of Active Ingredients from Traditional Chinese Medicine in Non-Small Cell Lung Cancer: A Meta-Analysis

Song Min[1], Tan Jinlong[2], Ding Silu[3], Liang Lixiang[4], Zhu Nailiang[5], Zhai Yingying[6], Wang Yajie[7*] and Chen Qiong[8*]

[1]College of Pharmacy, Xinyang Agricultural and Forestry University, Henan Xinyang 464000, China

[2]College of Pharmacy, Xinyang Agricultural and Forestry University, Henan Xinyang 464000, China

[3]College of Pharmacy, Xinyang Agricultural and Forestry University, Henan Xinyang 464000, China

[4]College of Pharmacy, Xinyang Agricultural and Forestry University, Henan Xinyang 464000, China

[5]College of Pharmacy, Xinyang Agricultural and Forestry University, Henan Xinyang 464000, China

[6]College of Pharmacy, Xinyang Agricultural and Forestry University, Henan Xinyang 464000, China

[7]Institute of Chinese Materia Medica, Chinese Academy of TCM, Beijing 100010, China

[8]College of Pharmacy, Xinyang Agricultural and Forestry University, Henan Xinyang 464000, China

***Corresponding author:**

Wang Yajie and Chen Qiong,
Institute of Chinese Materia Medica, Chinese Academy of TCM, Beijing 100010, China and College of Pharmacy, Xinyang Agricultural and Forestry University, Henan Xinyang 464000, China

Received: 08 May 2026
Accepted: 28 May 2026
Published: 05 June 2026
J Short Name: JTCM

Keywords:

Non-Small Cell Lung Cancer; Traditional Chinese Medicine; Active Ingredients; Apoptosis; Treatment Sensitization

Citation:

Wang Yajie and Chen Qiong, Therapeutic Efficacy and Molecular Mechanisms of Active Ingredients from Traditional Chinese Medicine in Non-Small Cell Lung Cancer: A Meta-Analysis. Jour of Tradi Chinese Med 2026; V3(1): 1-13

Abbreviation:

AD; Andrographolide**;** AS-IV: Astragaloside IV**;** CAG: Cycloastragenol**;** CI: Combination index; DRI: Dose-reduction index; ET: Effector-to-Target Ratio; EMT: Epithelial–Mesenchymal Transition; GS-Rd: Ginsenoside Rd; HLCSC: Human Lung Cancer Stem Cells; IC50: Half-Maximal Inhibitory Concentration; NK: Natural Killer; NSCLC: Non-Small Cell Lung Cancer; PA: Patchouli Alcohol; PDO: Patient-Derived Organoid; PDOX: Patient-Derived Organoid Xenograft; PPII: Polyphyllin II; PPVI: Polyphyllin VI; PTX; Paclitaxel; SERD0: Sensitizer Enhancement Ratio Based on D0; SF2: Surviving Fraction At 2 Gy; SNH: Sodium New Houttuyfonate; TIIA: Tanshinone IIA

1. Abstract

1.1. Background

Active ingredients derived from Traditional Chinese Medicine have been increasingly investigated as potential antitumor agents in non-small cell lung cancer (NSCLC). However, the available evidence is mainly preclinical and mechanistically heterogeneous, requiring structured synthesis.

1.2. Methods

A meta-analytic review was conducted on 24 included studies evaluating active TCM-derived ingredients in NSCLC models. Extracted outcomes included cytotoxicity, IC50 or IC-range values, apoptosis and regulated cell death responses, cell-cycle effects, treatment sensitization, resistance reversal, in vivo or advanced model evidence, and molecular pathway involvement.

1.3. Results

The evidence base was predominantly preclinical, using conventional NSCLC cell line models. Direct IC50 or IC-range data, while apoptosis or cell-death percentages were directly obtained. Several compounds showed measurable cytotoxicity, including bufalin, polyphyllin II, α-hederin, oridonin, honokiol, oxymatrine, chelerythrine chloride, patchouli alcohol, and ginsenoside Rd. Apoptosis-related mechanisms were the most frequent pathway category, followed by therapy sensitization, EMT/migration/invasion regulation, PI3K/Akt/mTOR-related signaling, and autophagy-related mechanisms. Combination and sensitization effects were observed for oridonin plus docetaxel, emodin plus paclitaxel, tanshinone IIA plus gefitinib, bufalin plus radiation, andrographolide plus anti-PD-1 therapy, and ginsenoside Rg3 plus cisplatin.

1.4. Conclusion

Active ingredients from Traditional Chinese Medicine exhibit multifaceted antitumor effects in NSCLC preclinical models, primarily through cytotoxicity, apoptosis induction, modulation of survival pathways, and treatment sensitization. Despite promising mechanistic and experimental evidence, future studies should prioritize standardized quantitative reporting and validation in patient-derived organoids, PDOX models, and clinically relevant combination-treatment systems.

2. Plain Language Summary

2.1. Why Did We Do This Study?

Non-small cell lung cancer (NSCLC) often stops responding to standard treatments. Scientists have looked at natural compounds from Traditional Chinese Medicine (TCM) as possible helpers. But no one had yet combined all the available lab evidence to see what really works and how.

2.2. What Did We Do?

We analyzed 24 laboratory studies that tested pure TCM ingredients (such as bufalin, ginsenosides, and tanshinone) in NSCLC cells and animal models. We asked: Do these compounds kill cancer cells? Can they make standard therapies work better?

2.3. What Did We Find?

Many TCM ingredients killed NSCLC cells or stopped their growth, mainly by triggering apoptosis – a natural self-destruct process inside cells.

Several compounds also boosted the effects of chemotherapy, targeted drugs, radiation, and immunotherapy. For example, tanshinone IIA helped overcome resistance to the drug gefitinib, and bufalin made lung cancer cells more sensitive to radiation.

However, almost all studies used lab-grown cells or animals, not human patients. Only one study used patient-derived mini-tumors (organoids).

2.4. What Do These Results Mean?

These natural compounds show real promise, especially as add-ons to existing cancer treatments. But they are not ready for patient use. Future research must test the most promising ingredients in human trials using consistent methods.

2. Introduction

Non-small cell lung cancer (NSCLC) remains a major therapeutic challenge because tumor progression, metastatic capacity, treatment resistance, and recurrence are driven by multiple interacting molecular pathways rather than by a single dominant oncogenic process [1]. Although chemotherapy, radiotherapy, molecularly targeted therapy, and immunotherapy have improved disease control in selected patient groups, resistance to paclitaxel, cisplatin, gefitinib, osimertinib, anlotinib, and immune-based treatment remains a persistent experimental and clinical concern [2,3]. This has increased interest in bioactive compounds capable of simultaneously modulating proliferation, apoptosis, invasion, autophagy, oxidative stress, stemness, and treatment sensitivity.

Active ingredients derived from Traditional Chinese Medicine (TCM) have been widely investigated as potential antitumor agents in NSCLC models. The included experimental literature shows that several compounds suppress NSCLC cell viability and proliferation across diverse cell lines, including A549, H460, H1299, PC-9, HCC827, NCI-H1975, H358, H520, H1650, 95-D, SK-LU-1, and resistant A549/V16 models [4-6]. Reported cytotoxic effects span nanomolar activity for bufalin and triptolide-related models, micromolar activity for compounds such as oridonin, honokiol, chelerythrine chloride, polyphyllin II, α-hederin, and patchouli alcohol, and higher-dose responses for oxymatrine and ginsenoside Rd [7-11]. These findings suggest that TCM-derived active ingredients represent a heterogeneous but biologically active compound class in preclinical NSCLC research.

A central mechanism reported across these studies is the induction of apoptosis and regulated cell death. Triptolide, honokiol, osthole, oxymatrine, astragaloside IV, emodin, ellagic acid, bufalin, polyphyllin II, patchouli alcohol, ginsenoside Rd, ginsenoside Rg3, and cycloastragenol have been associated with apoptosis-related signaling through caspase activation, mitochondrial regulation, p53-associated pathways, Bax/Bcl-2 modulation, or cell-cycle disruption [12-15]. Other studies extend this mechanistic spectrum to pyroptosis and inflammasome activation, particularly through polyphyllin VI and sodium new houttuyfonate, and to autophagy or lysosomal dysfunction through honokiol, polyphyllin II, andrographolide, α-hederin, and cycloastragenol [3, 13, 16-19]. Therefore, TCM active ingredients may influence NSCLC via multiple forms of regulated cell death rather than solely through apoptosis.

Treatment sensitization is another important theme. Oridonin showed synergistic interaction with docetaxel, emodin enhanced paclitaxel activity, tanshinone IIA reversed gefitinib resistance, patchouli alcohol retained activity in vincristine-resistant NSCLC cells, bufalin enhanced radiosensitivity, andrographolide potentiated anti-PD-1-related antitumor immunity, and ginsenoside Rg3 improved cisplatin-response assessment in patient-derived organoid models [2, 7, 9, 20]. These studies indicate that several TCM-derived compounds may be more relevant as adjuvants or sensitizers than as isolated cytotoxic monotherapies.

Mechanistically, the included studies implicate several recurrent pathway families, including EGFR/ERK/MMP-12 and CIP2A/Akt signaling, Akt/GSK-3β/β-catenin regulation, PI3K/Akt and PI3K/Akt/mTOR signaling, AXL downregulation, HAS2–HA–CD44/RHAMM signaling, ULBP1/DR5-mediated immune susceptibility, miRNA- and lncRNA-mediated regulation, ROS-associated DNA damage, and SMYD2- or AMPK/ULK1/mTOR-related mechanisms [20-24]. However, the evidence remains highly heterogeneous across compound type, cell model, dose, exposure time, endpoint definition, and reporting completeness. A structured meta-analytic synthesis is therefore needed to organize the available preclinical evidence, identify the strongest quantitative outcome domains, and clarify the major molecular mechanisms through which TCM active ingredients act in NSCLC models.

3. Methods

3.1. Study Design and Reporting Framework

This study was designed as a systematic review and meta-analysis evaluating the therapeutic efficacy and molecular mechanisms of active ingredients derived from Traditional Chinese Medicine in non-small cell lung cancer (NSCLC). The review

was conducted and reported according to the Preferred Reporting Items for Systematic Reviews and Meta-Analyses (PRISMA) 2020 statement. The study question was structured around the following framework: population/model, NSCLC; intervention, a clearly defined active ingredient derived from Traditional Chinese Medicine; comparator, untreated, vehicle, negative, standard-treatment, or disease-control group; outcomes, quantitative efficacy and mechanistic endpoints.

3.2. Literature Search Strategy

A systematic search was conducted for studies published from January 2015 to 2026. PubMed/MEDLINE, Scopus, Web of Science Core Collection, Embase, Cochrane Library, and Google Scholar were searched using combinations of terms related to NSCLC, Traditional Chinese Medicine, active ingredients, natural compounds, and anticancer mechanisms. The main search concepts included: "non-small cell lung cancer", "NSCLC", "lung adenocarcinoma", "Traditional Chinese Medicine", "Chinese herbal medicine", "active ingredient", "bioactive compound", "natural product", "phytochemical", "apoptosis", "autophagy", "cell cycle", "migration", "invasion", "tumor growth", "drug resistance", and molecular pathways including PI3K/Akt, MAPK, NF-κB, STAT3, Wnt/β-catenin, EGFR, VEGF, p53, Bax/Bcl-2, caspase, and EMT. The reference lists of eligible articles and relevant reviews were also manually screened.

3.3. PRISMA-Based Study Selection

The study-selection process was conducted according to the PRISMA 2020 framework, and the complete identification, screening, eligibility, and inclusion process is presented in Figure 1.

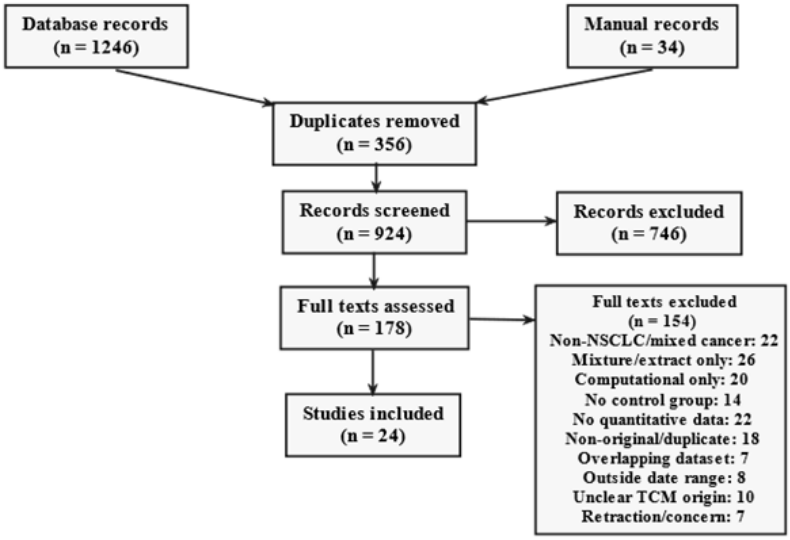

Figure 1: PRISMA 2020 flow diagram of study identification, screening, eligibility assessment, and final inclusion.

3.4. Eligibility Criteria

Studies were included if they met all of the following criteria: original experimental or clinical study; publication between January 2015 and 2026; English full-text availability; NSCLC-specific model or patient population; evaluation of a clearly defined active ingredient derived from Traditional Chinese Medicine; presence of a control or comparator group; availability of quantitative data suitable for extraction; and reporting of at least one therapeutic or mechanistic outcome.

Studies were excluded if they were reviews, meta-analyses, editorials, letters, protocols, conference abstracts, patents, or book chapters; investigated small-cell lung cancer or mixed cancer populations without extractable NSCLC data; evaluated crude herbal formulas, decoctions, extracts, fractions, or multi-compound mixtures without separable active-ingredient data; used only network pharmacology, molecular docking, molecular dynamics, or bioinformatics prediction without experimental or clinical validation; lacked a control group; lacked extractable quantitative data; duplicated another dataset; or had a confirmed retraction notice.

3.5. Outcomes

The primary quantitative outcomes were anticancer efficacy endpoints, including cell viability or proliferation, apoptosis or cell-death rate, migration and invasion inhibition, tumor volume, tumor weight, and treatment response where clinical data were available. Secondary outcomes included chemosensitivity, radiosensitivity, drug-resistance reversal, cell-cycle arrest, autophagy, ferroptosis, pyroptosis, oxidative-stress markers, and quantitative expression of mechanistic biomarkers.

Mechanistic outcomes were grouped by pathway or biological process, including PI3K/Akt/mTOR, MAPK/ERK, NF-κB, STAT3/JAK, Wnt/β-catenin, EGFR-related signaling, VEGF/angiogenesis, p53-mediated apoptosis, Bax/Bcl-2/caspase activation, EMT regulation, oxidative-stress signaling, metabolic reprogramming, autophagy, ferroptosis, pyroptosis, and immune-modulatory pathways.

3.6. Data Extraction

Data were extracted independently by two reviewers using a standardized extraction sheet. Extracted variables included first author, publication year, active ingredient, TCM source where

reported, NSCLC cell line or clinical population, experimental model, comparator, dose or concentration, exposure duration, sample size, outcome type, mean value, standard deviation or standard error, event counts, effect estimates, mechanistic markers, and major pathway findings. When numerical data were available only in figures, values were extracted using digital graph-extraction methods. Standard error, confidence interval, or interquartile range data were converted to standard deviation when appropriate.

3.7. Risk of Bias and Methodological Quality Assessment

Methodological quality was assessed based on the study design. In vivo animal studies were evaluated using domains adapted from the SYRCLE risk-of-bias tool. In vitro studies were assessed for cell-line definition, control adequacy, dose reporting, exposure duration, replication, outcome measurement, and selective reporting. Clinical studies, if eligible, were assessed using the Cochrane risk-of-bias tool for randomized studies or ROBINS-I for non-randomized studies. Studies with major concerns regarding retraction status, duplicate publication, absent controls, or non-extractable outcomes were excluded from quantitative synthesis.

3.8. Statistical Analysis

Meta-analysis was performed only when at least three independent studies reported comparable quantitative outcomes. Continuous outcomes were pooled as mean differences when measured on the same scale and as standardized mean differences when measured on different scales. Binary outcomes were pooled as risk ratios or odds ratios. Survival outcomes, where available, were summarized using hazard ratios. All pooled estimates were reported with 95% confidence intervals.

A random-effects model was used as the primary model because heterogeneity was expected across compounds, cell lines, experimental platforms, doses, and outcome measurements. Statistical heterogeneity was assessed using the I^2 statistic and Cochran's Q test. Subgroup analyses were planned according to active ingredient class, experimental model, NSCLC cell line, treatment type, and outcome category. Sensitivity analysis was performed by excluding studies with a high risk of bias, studies with graph-extracted data, or studies with extreme effect sizes. Publication bias was assessed by funnel plot and Egger's test when at least ten studies were available for a given outcome. Outcomes with fewer than three comparable studies were synthesized narratively rather than pooled statistically.

3.9. Evidence Synthesis

The final synthesis integrated quantitative efficacy findings with mechanistic evidence. Pooled outcomes were presented separately for proliferation/viability, apoptosis, migration/invasion, tumor burden, chemosensitization/radiosensitization, and resistance reversal. Mechanistic results were summarized by signaling pathway and biological function to identify the most consistently reported molecular targets of TCM-derived active ingredients in NSCLC.

4. Results

4.1. Study Characteristics and Evidence Map

The final evidence base comprised 24 included studies evaluating active ingredients of Traditional Chinese Medicine in NSCLC models. As summarized in Table 1 and Figure 2A, the dataset was predominantly preclinical, with all studies using in vitro cellular or organoid-based experimental systems. Most studies (23 of 24; 95.8%) were conducted in conventional 2D NSCLC cell line models, whereas one study (4.2%) used patient-derived organoid models. Year-reportable studies covered a publication window from 2016 to 2026, with a median publication year of 2020, indicating that the dataset was concentrated in relatively recent experimental literature.

The included studies used a broad range of NSCLC models, including A549, H460, H1299, PC-9, HCC827, NCI-H1975, H358, H520, H1650, 95-D, SK-LU-1, HLCSC, A549/V16, and patient-derived lung adenocarcinoma organoids. Treatment conditions varied substantially across compounds, with concentrations ranging from nanomolar levels for bufalin and triptolide to micromolar or millimolar levels for several other active ingredients. Exposure durations also differed by endpoint, ranging from 24–72 h for most viability and apoptosis assays to longer colony-formation, xenograft, and organoid-based protocols.

Figure 2B shows that directly reported IC50 or IC-range data were available in 13 studies (54.2%), making cytotoxic potency one of the strongest quantitative domains in the dataset. Animal, xenograft, or advanced-model evidence was reported in 9 studies (37.5%), and 8 studies (33.3%) included therapeutic animal experiments. Combination-treatment, resistance-reversal, immune-sensitization, or radiosensitization designs were also present in 8 studies (33.3%), supporting the need to analyze these studies separately from single-agent cytotoxicity experiments. Directly reported apoptosis or cell-death percentages were available in 6 studies (25.0%).

Table 1: Core characteristics of the 24 included studies.

Ref.	Active ingredient	Main model/ cell line(s)	Main treatment range or key dose	Main exposure or follow-up	Numerical design details
[1]	Triptolide	PC-9	0, 10, 25, 50 nM	Viability 3 days; apoptosis/ mechanism 2 days	MTT 1 × 10^4 cells/well; apoptosis/ western blot 1 × 10^6 cells/well
[2]	Oridonin	A549; NCI-H1975	0–20 μM; in vivo 30 mg/kg	In vitro 24 h; xenograft 3 weeks	Xenograft: 2.5 × 10^6 H1975 cells; Ori n=8, gefitinib n=7, vehicle n=7
[3]	Honokiol	H460, A549, H358	0–80 μM	Viability 72 h; apoptosis 48 h; colony 10–14 days	Viability 3 × 10^3 cells/well; colony 500 cells/well; apoptosis triplicate

[4]	Osthole	A549	Osthole 100 μM; embelin 50 μM; osthole 0–150 μM	24 h	Viability 5 × 10^3 cells/well; apoptosis/western blot 5 × 10^5 cells/well
[5]	Oxymatrine		0.25–5 mM; selected 0.5 and 1 mM		Viability N=3; apoptosis/caspase/cell-cycle/EMT panels N=4
[6]	Astragaloside IV	A549, HCC827, NCI-H1299	3, 6, 12, 24 ng/mL	Proliferation/apoptosis 48 h; migration 24 h	Mean ± SEM from 3 independent experiments
[7]	Emodin + PTX	A549; A549 xenograft	Emodin 0–120 μM; PTX 0–32 μM; in vivo 50 mg/kg + 10 mg/kg PTX	In vitro 72 h; in vivo 3 weeks	Xenograft 16 mice total; 4 mice/group; 5 × 10^6 A549 cells
[8]	Honokiol	A549	Screening 0–100 μM; selected 45 μM	24–48 h; selected 48 h	CCK-8/apoptosis 5 repeats/group; RNA-seq 3 samples/group
[9]	Tanshinone IIA + gefitinib	HCC827/gefitinib; PC-9/gefitinib	TIIA 0–16 μM; gefitinib 0–320 nM; in vivo TIIA 20 mg/kg + gefitinib 150 mg/kg	Viability 72 h; migration/invasion 24 h; in vivo 3 weeks	In vivo n=16 mice, 4 groups
[10]	Chelerythrine chloride	NCI-H1703, SK-LU-1, HLCSC	0.75–6 μg/mL; kinetic range 1.56–50 μg/mL	24, 48, 72 h; migration/invasion 16 h; soft agar 3 weeks	Dose-response duplicate data in 2 independent experiments; migration/invasion 3 independent experiments
[11]	Ellagic acid	A549	5, 10, 20 μM	48 h	n=3 for MTT, cell cycle, apoptosis, and western blot figures
[12]	Bufalin	A549, H460	20, 40, 80 nM	Viability 24/48 h; colony 7–10 days; promoter 4/8 h	Triplicate samples or ≥3 independent experiments
[13]	Polyphyllin VI	A549, H1299; A549 xenograft	PPVI 4/6 μM in vitro; 2.5, 5, 10 mg/kg in vivo	In vitro 24–72 h; in vivo 10 days	In vivo 5 groups, 8 mice/group
[14]	Emodin	A549, H520, H1975, H1299, H460	1–30 μM; selected 30 μM	24 h	Viability 4 × 10^3 cells/well; apoptosis 3–5 × 10^3 cells/well
[15]	Tanshinone IIA	A549, H460, H1299, Fluc+ A549; H460/LLC models	0.156–10 μM; in vivo TIIA-SS 0.5 mg/kg	MTT 24–72 h; H460 sacrifice day 18; LLC sacrifice day 23	NK transfer 1 × 10^7 cells on days 1, 8, 15; H460 inoculation 3 × 10^6 cells; LLC inoculation 1.5 × 10^6 cells
[16]	Polyphyllin II	A549, H1299	0, 1, 5, 10 μM; CQ 10 μM; 3-MA 5 mM	24 h	Replication/sample size not reported in text-readable notes
[17]	Andrographolide	H1975, H1299, H1650, H460; H1975 xenograft; Lewis lung carcinoma	AD 2.5, 5, 10 mg/kg in vivo; AD 5 mg/kg + anti-PD-1 10 mg/kg	21 days in vivo; tumor measured every 3 days	H1975 inoculation 5 × 10^5 cells; anti-PD-1 model 28 mice, 7/group; starting tumor volume 50 ± 7 mm^3
[18]	Sodium new houttuyfonate	NCI-H1299, NCI-H23, A549, SK-MES-1, NCI-H2170; orthotopic model	SNH 0, 0.1, 0.2, 0.4 mM; in vivo 37.5 mg/kg/day	In vivo 21 days	Orthotopic model 3 groups, n=10/group; TCONS-14036 lentivirus 1 × 10^6 cells
[19]	Patchouli alcohol	A549, A549/V16, SVEC	PA 3.3–135 μM; cisplatin 3.3–53.1 μM	Viability 24/48 h; colony 48 h + 7 days	IC60 selected: 112 μM for A549 and 135 μM for A549/V16
[21]	Bufalin + radiation	A549, H1299, HCC827	Bufalin 0–200 nM; radiation 2, 4, 6 Gy	Viability 24–72 h; radiation assays 48 h; clonogenic 2 weeks	Clonogenic seeding 1000 cells/well; X-rays 6 MV at 4 Gy/min
[22]	Ginsenoside Rd	95-D, NCI-H460	50, 100, 200 μg/mL; DOX 5 μM	Proliferation 24/48/72 h; migration 72 h; colony 21 days	n≥3; 5 parallel wells/concentration; western blot protein 60 μg/lane
[23]	Alpha-hederin	H1299, A549	4, 8, 16 μM; CQ 20 μM	Main treatment 24 h	CCK-8 1000 cells/well; colony 800 cells/well; transwell 2 × 10^4 cells/well
[20]	Ginsenoside Rg3 + cisplatin	3 lung adenocarcinoma PDO lines; PDOX model	0.001, 0.01, 0.1, 1, 10, 50 μM; cisplatin:Rg3 = 1:1, 2:1, 4:1	Drug treatment 48 h	3 replicate wells/condition; PDOX 6 mice across 2 PDO lines; negative control 3 mice
[24]	Cycloastragenol	H1299, A549; A549 xenograft	0, 25, 50, 75 μmol/L; in vivo 150 mg/kg/day	Apoptosis 72 h; xenograft sacrifice day 17	Colony 500 cells/well; xenograft 3 × 10^6 A549 cells; in vivo n=7/group

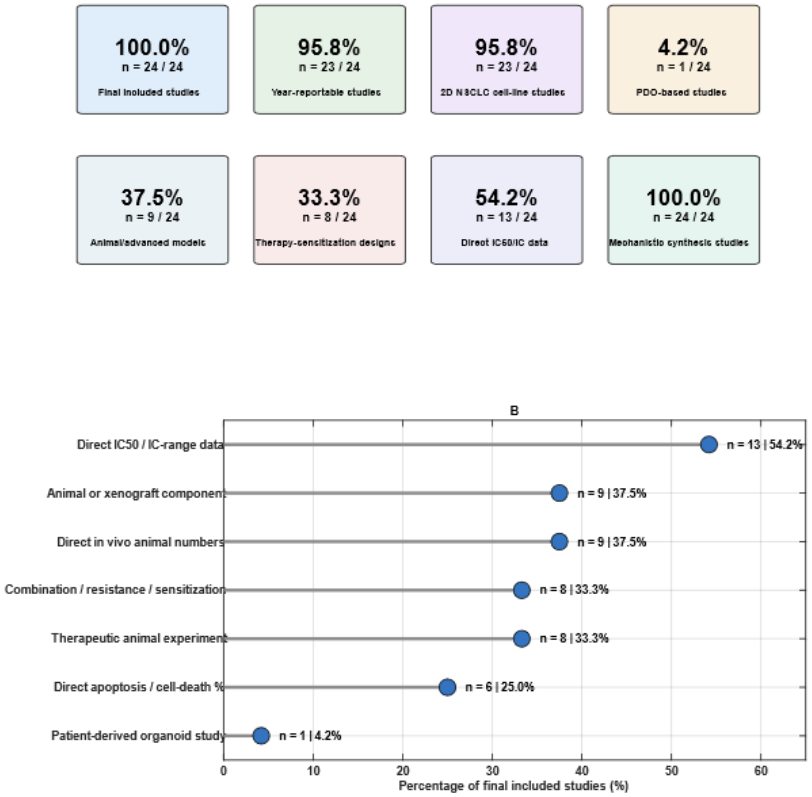

Figure 2: Evidence-map profile of the final included studies. A: Overall composition and study-design profile of the 24 included studies. B: Availability of key quantitative and advanced preclinical evidence across the final dataset.

4.2. Cytotoxicity, Proliferation Inhibition, and IC50-Based Potency

Directly reported IC50 and IC-range data were available across multiple NSCLC models, supporting a quantitative comparison of cytotoxic potency and treatment-sensitization patterns. As shown in Figure 3A, IC50 values in the μM-scale studies varied substantially across compounds and cell models. Among the directly comparable μM-scale data, polyphyllin II showed the lowest IC50 in H1299 cells (2.86 μM), followed by polyphyllin II in A549 cells (8.26 μM) and α-hederin in A549 cells (14.22 μM). Oridonin also showed stronger cytotoxicity in NCI-H1975 cells than in A549 cells, with IC50 values of 15.53 μM and 55.91 μM, respectively. Patchouli alcohol showed higher IC50 values in A549 and A549/V16 cells, whereas the highest IC50 in this subset was observed in SVEC normal cells (167.31 μM), supporting a degree of cancer-cell selectivity in that study.

Nanomolar potency was most evident in the bufalin- and gefitinib-based sensitization models (Figure 3B). Bufalin showed low-nanomolar IC50 values in A549 and H460 cells, with an approximate IC50 of 30 nM across multiple NSCLC cell lines. In resistant EGFR-mutant models, tanshinone IIA markedly enhanced gefitinib sensitivity, reducing the gefitinib IC50 from 172.20 to 42.37 nM in HCC827/gefitinib cells and from 167.00 to 75.77 nM in PC-9/gefitinib cells. These reductions indicate that the cytotoxic effect extended beyond baseline growth inhibition to targeted-therapy resistance reversal.

Time-dependent IC50 patterns further differentiated compounds with stable potency from those showing exposure-dependent enhancement (Figure 3C). Chelerythrine chloride maintained relatively stable IC50 values over 24–72 h in NCI-H1703 and SK-LU-1 cells, while HLCSC cells showed a gradual increase in IC50 over time. In contrast, ginsenoside Rd demonstrated a strong time-dependent decrease in IC50, particularly in 95-D cells, where the IC50 declined from 867.10 μg/mL at 24 h to 80.60 μg/mL at 72 h. NCI-H460 cells were consistently more sensitive to ginsenoside Rd than 95-D cells across all assessed time points.

Combination and sensitization effects were also quantitatively evident (Figure 3D). Emodin reduced the paclitaxel IC50 in a concentration-dependent manner, with the greatest reduction observed at 40 μM. Tanshinone IIA also produced substantial gefitinib IC50 reductions in both resistant cell models, with the larger fold-reduction observed in HCC827/gefitinib cells.

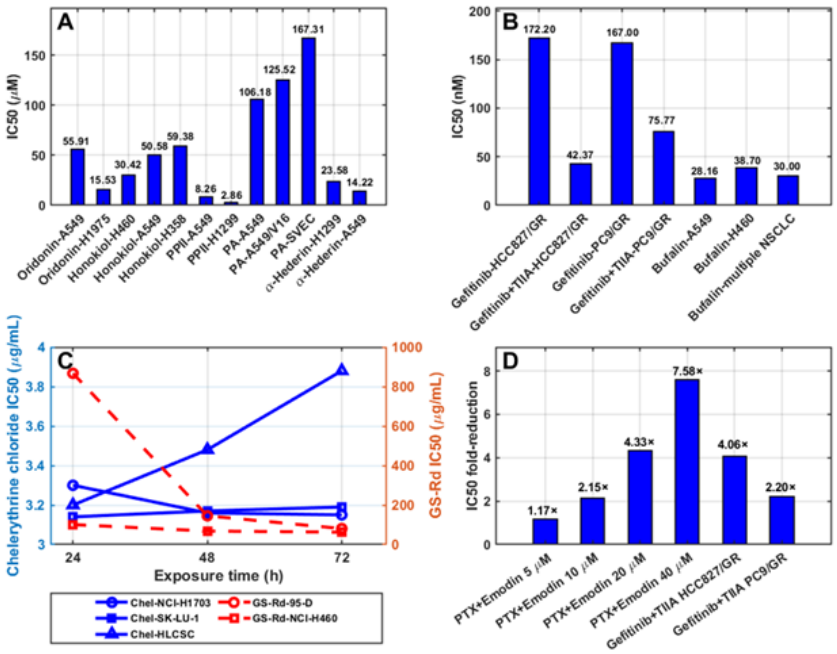

Figure 3: IC50-based potency and treatment-sensitization profile across directly reported cytotoxicity studies. A: IC50 values reported in μM-scale models. B: IC50 values reported in nM-scale targeted-therapy and bufalin models. C: Time-dependent IC50 changes for chelerythrine chloride and ginsenoside Rd. D: Fold-reduction of IC50 after combination or sensitizing treatment.

4.3. Apoptosis, Cell-Cycle Arrest, and Regulated Cell-Death Responses

Direct percentage-based outcomes showed that several active ingredients induced regulated cell death or suppressed cell viability in NSCLC models. As shown in Figure 4A, osthole increased apoptosis in A549 cells from 4.26 ± 0.41% in the control group to 18.31 ± 2.67%, while embelin increased apoptosis to 14.76 ± 1.05%. The combined osthole–embelin treatment produced the strongest apoptotic response, reaching 34.36 ± 2.98%, corresponding to an 8.07-fold increase compared with control and a 1.88-fold increase compared with osthole alone.

Oxymatrine produced a clear dose-dependent reduction in A549 cell viability (Figure 4B). Viability declined from 80.38% at 0.5 mM to 51.25% at 1 mM, 27.66% at 2 mM, 13.74% at 2.5 mM, and 2.31% at 5 mM. This corresponded to progressive growth inhibition from 19.62% to 97.69%, with the 1 mM concentration approximating the reported IC50 level. Oxymatrine also increased early apoptosis from 2.46% to 5.59% and late apoptosis from 6.20% to 8.84% at 1 mM, indicating that viability loss was accompanied by apoptotic activation.

Immune-mediated cytotoxicity was represented by tanshinone IIA-enhanced NK-cell lysis (Figure 4C). At an effector-to-target ratio of 1:1, 10 μM tanshinone IIA increased NK-mediated lysis from 15.2% to 22.7% in A549 cells, from 10.2% to 20.0% in H460 cells, from 10.2% to 25.0% in H1299 cells, and from 31.7% to 60.9% in Fluc+ A549 cells. The largest relative increase among conventional 2D NSCLC cell lines was observed in H1299 cells, whereas the highest absolute lysis level was observed in Fluc+ A549 cells.

Patchouli alcohol produced marked cell-death effects in both parental and vincristine-resistant NSCLC cells (Figure 4D). The subG1 population increased from 5.14 ± 1.30% to 44.35 ± 5.45% in A549 cells and from 5.88 ± 2.24% to 41.34 ± 4.92% in A549/V16 cells. Similarly, TUNEL-positive apoptosis increased from 4.14 ± 2.48% to 50.37 ± 8.35% in A549 cells and from 4.63 ± 1.57% to 43.30 ± 8.87% in A549/V16 cells, supporting the preservation of pro-apoptotic activity in the resistant model.

Ginsenoside Rd was associated with cell-cycle redistribution and strong antiproliferative activity (Figure 4E). S-phase accumulation increased from 25.16 ± 0.37% to 38.42 ± 0.29%, while the reported overall apoptosis and proliferation-inhibition values were approximately 54.85% and 99.52%, respectively. The effect-index summary in Figure 4F further highlights that the most pronounced direct percentage-based responses were observed for patchouli alcohol-induced TUNEL apoptosis, osthole–embelin-induced apoptosis, and tanshinone IIA-enhanced NK-mediated lysis.

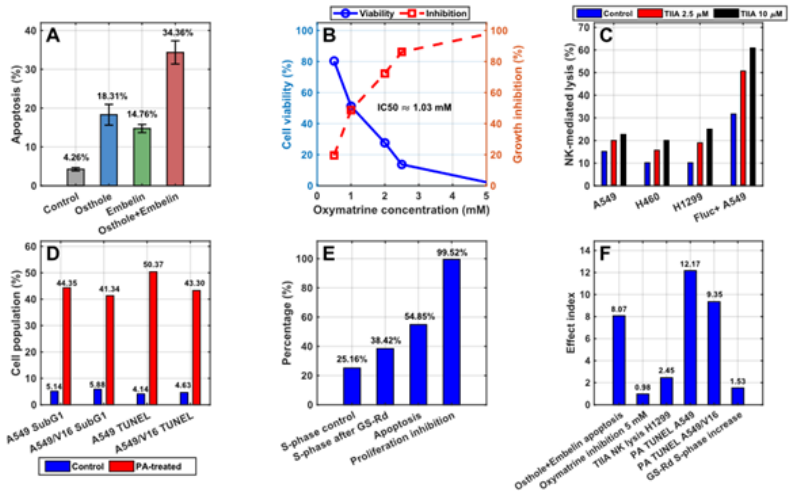

Figure 4: Directly reported cytotoxic, apoptotic, immune-killing, and cell-cycle outcomes. A: Osthole/embelin-induced apoptosis in A549 cells. B: Oxymatrine dose-dependent viability reduction in A549 cells. C: Tanshinone IIA-enhanced NK-mediated lysis across NSCLC models. D: Patchouli alcohol-induced subG1 accumulation and TUNEL apoptosis in parental and vincristine-resistant NSCLC cells. E: Ginsenoside Rd-associated S-phase arrest, apoptosis, and proliferation inhibition.

4.4. Chemosensitization, Resistance Reversal, Immunosensitization, and Radiosensitization

Treatment-sensitization outcomes showed that several active ingredients enhanced the activity of conventional chemotherapy, targeted therapy, immune-mediated cytotoxicity, or radiation. As shown in Figure 5A, all reported oridonin–docetaxel combinations had combination index values below 1.0, indicating synergistic interactions. The strongest was observed for oridonin 2.5 μM plus docetaxel 8 nM, with a CI of 0.22, followed by oridonin 2.5 μM plus docetaxel 4 nM (CI = 0.32), oridonin 5 μM plus docetaxel 8 nM (CI = 0.39), and oridonin 5 μM plus docetaxel 4 nM (CI = 0.52).

of immune- and PDO-based sensitization studies.

Chemosensitization and targeted-therapy resistance reversal were also evident from IC50 fold-reduction metrics (Figure 5B). Emodin reduced the paclitaxel IC50 by 2.15-fold at 10 μM and by 4.33-fold at 20 μM, indicating a concentration-dependent enhancement of paclitaxel activity. Tanshinone IIA similarly improved gefitinib responsiveness in resistant EGFR-mutant NSCLC models, with a 4.06-fold IC50 reduction in HCC827/gefitinib cells and a 2.20-fold reduction in PC-9/gefitinib cells.

Radiosensitization was represented by the bufalin–radiation experiments (Figure 5C). In A549, H1299, and HCC827 cells, bufalin combined with radiation reduced SF2 compared with radiation alone, yielding SERD0 values of 1.19, 1.28, and 1.42, respectively. The largest radiosensitizing effect was observed in HCC827 cells, where SERD0 reached 1.42, and SF2 decreased from 0.89 to 0.59.

Immune- and organoid-based sensitization evidence was more limited but experimentally important (Figure 5D). The immune-sensitization studies included three NK-cell administrations in the tanshinone IIA model and an anti-PD-1 combination design with seven mice per group in the andrographolide study. The organoid-based ginsenoside Rg3/cisplatin study evaluated three PDO lines, three drug-ratio conditions, and six concentration levels, with two of the three PDO lines favoring the 4:1 cisplatin: Rg3 ratio.

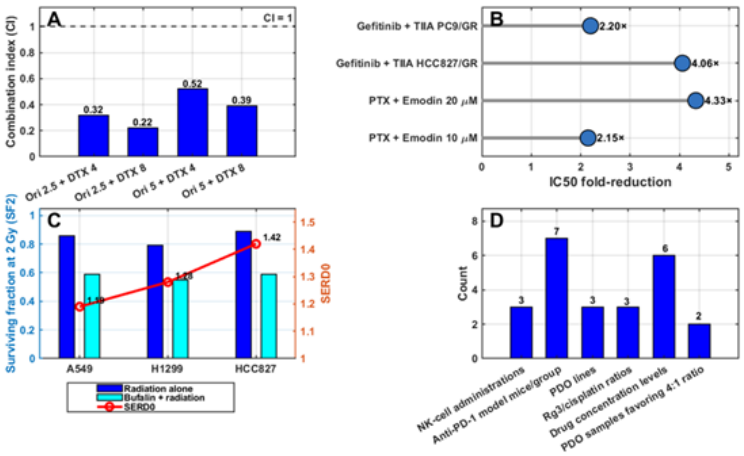

Figure 5: Treatment-sensitization, resistance-reversal, and radiosensitization metrics. A: Combination-index profile for oridonin plus docetaxel. B: IC50 fold-reduction after emodin/paclitaxel and tanshinone IIA/gefitinib combinations. C: Bufalin-mediated radiosensitization across NSCLC cell lines. D: Experimental design intensity of immune- and PDO-based sensitization studies.

4.5. In Vivo, Organoid, and Advanced Preclinical Model Evidence

Advanced preclinical evidence was identified across xenograft, orthotopic, immune-competent, patient-derived organoid, and PDOX models. As summarized in Table 2, in vivo validation was reported for several treatment contexts, including direct antitumor activity, chemosensitization, reversal of targeted-therapy resistance, pyroptosis-related tumor inhibition, immune-mediated antitumor activity, and organoid-based chemosensitivity assessment.

Xenograft studies provided the main in vivo evidence for antitumor efficacy and treatment sensitization. Oridonin was evaluated in an H1975 xenograft model using 30 mg/kg treatment over 3 weeks, supporting in vivo validation in a gefitinib-resistant NSCLC context. Emodin was assessed in an A549 xenograft model in combination with paclitaxel, using 50 mg/kg emodin and 10 mg/kg paclitaxel over 3 weeks in 16 mice. Tanshinone IIA was tested in an HCC827/gefitinib xenograft model with gefitinib 150 mg/kg and tanshinone IIA 20 mg/kg for 3 weeks, providing in vivo evidence for reversal of EGFR-TKI resistance.

Pyroptosis- and ncRNA-related mechanisms were supported by advanced animal models. Polyphyllin VI was evaluated in an A549 xenograft model using three in vivo doses (2.5, 5, and 10 mg/kg) and gefitinib as a positive control, with 8 mice per group over a 10-day treatment period. Sodium new houttuyfonate was assessed in an orthotopic NSCLC model using oral administration at 37.5 mg/kg/day for 21 consecutive days, with 10 mice per group, supporting in vivo validation of the TCONS-14036/miR-1228-5p/PRKCDBP-related pyroptosis axis.

Tanshinone IIA and andrographolide represented immune-related advanced models. Tanshinone IIA was examined in an H460 SCID-Bg xenograft model with NK-cell transfer, using 1 × 10^7 NK cells administered on days 1, 8, and 15, and in an LLC syngeneic model with NK-depletion experiments. Andrographolide was evaluated in an H1975 xenograft model using 2.5, 5, and 10 mg/kg daily dosing and in a Lewis lung carcinoma model combined with anti-PD-1 therapy, with 28 mice allocated across 4 groups and a starting tumor volume of 50 ± 7 mm3.

The most clinically advanced experimental platform was represented by the ginsenoside Rg3/cisplatin study, which used 3 lung adenocarcinoma patient-derived organoid lines and a PDOX characterization model. The organoid component tested three cisplatin: Rg3 ratios across six concentration levels, with three replicate wells per condition, while the PDOX model included 2 PDO lines and 6 mice in total. Cycloastragenol was also evaluated in an A549 xenograft model using 150 mg/kg/day treatment, 3 × 10^6 A549 cells inoculated, and 7 mice per group, with sacrifice on day 17.

Table 2: In vivo, organoid, and advanced-model evidence.

Ref.	Advanced model	Compound/treatment	Key numerical design	Treatment duration or endpoint	Main Results use
[2]	H1975 xenograft	Oridonin 30 mg/kg; gefitinib 30 mg/kg	H1975 inoculum 2.5 × 10^6 cells; Ori n=8, gefitinib n=7, vehicle n=7	3 weeks	In vivo validation of gefitinib-resistant NSCLC inhibition
[7]	A549 xenograft	Emodin 50 mg/kg + PTX 10 mg/kg	16 mice total; 4 mice/group; A549 inoculum 5 × 10^6 cells		In vivo chemosensitization evidence
[9]	HCC827/gefitinib xenograft	Gefitinib 150 mg/kg + TIIA 20 mg/kg	n=16 mice; 4 groups; starting tumor volume ~200 mm^3		In vivo gefitinib-resistance reversal
[13]	A549 xenograft	PPVI 2.5, 5, 10 mg/kg; gefitinib 20 mg/kg	5 groups; 8 mice/group; A549 inoculum 1 × 10^6 cells/mouse	10 days	In vivo NLRP3 inflammasome/pyroptosis evidence
[15]	H460 SCID-Bg xenograft	TIIA-SS 0.5 mg/kg + NK transfer	H460 inoculum 3 × 10^6 cells; NK cells 1 × 10^7 on days 1, 8, 15	Sacrifice day 18	NK-cell immunosensitization evidence
	LLC syngeneic model	TIIA-SS 0.5 mg/kg; NK-depletion experiment	LLC inoculum 1.5 × 10^6 cells	Sacrifice day 23	Immune-competent antitumor validation
[17]	H1975 xenograft	AD 2.5, 5, 10 mg/kg daily	H1975 inoculum 5 × 10^5 cells; tumor measured every 3 days	21 days	Dose-dependent in vivo tumor-growth suppression
	Lewis lung carcinoma + anti-PD-1	AD 5 mg/kg daily + anti-PD-1 10 mg/kg twice weekly	28 mice; 7/group; start tumor volume 50 ± 7 mm^3		Immunotherapy potentiation and CD8+ T-cell activation

[18]	Orthotopic NSCLC model	SNH 37.5 mg/kg/day orally	3 groups; n=10/group; TCONS-14036 lentivirus 1 × 10^6 cells	21 consecutive days	In vivo pyroptosis/ncRNA-axis validation
[20]	Lung adenocarcinoma PDO	Rg3 + cisplatin	3 PDO lines; 3 replicate wells/condition; organoid diameter 20–50 µm	48 h drug exposure	Patient-derived chemosensitivity platform
	PDOX characterization	Lung adenocarcinoma organoid-derived xenograft	2 PDO lines; 3 mice/line; 6 mice total; negative-control mice n=3	Tumor dimensions twice weekly	Model fidelity and advanced preclinical validation
[24]	A549 xenograft	Cycloastragenol 150 mg/kg/day	A549 inoculum 3 × 10^6 cells; n=7/group	Sacrifice day 17	In vivo antitumor activity and biosafety assessment

4.6. Molecular Mechanisms and Pathway-Level Synthesis

The mechanistic synthesis showed substantial biological heterogeneity across the 24 included studies, with multiple overlapping pathways contributing to the antitumor effects of active ingredients from Traditional Chinese Medicine. As shown in Figure 6, apoptosis-related mechanisms were the most frequently reported pathway category, appearing in 13 studies (54.2%). This dominant group included mitochondrial apoptosis, caspase activation, p53-related signaling, and apoptosis-associated modulation of Bax, Bcl-2, cleaved caspase-3, and related cell-death markers.

Therapy sensitization was the second most frequent mechanistic domain, reported in 8 studies (33.3%). These studies covered chemosensitization, EGFR-TKI resistance reversal, immune-related sensitization, and radiosensitization. The evidence included oridonin–docetaxel synergy, emodin-mediated enhancement of paclitaxel activity, tanshinone IIA-mediated reversal of gefitinib resistance, bufalin-mediated radiosensitization, andrographolide combined with anti-PD-1 therapy, and ginsenoside Rg3 combined with cisplatin in patient-derived organoids.

Mechanisms related to EMT, migration, invasion, and metastasis regulation were reported in 7 studies (29.2%), while PI3K/Akt/mTOR or Akt-related signaling was reported in 6 studies (25.0%). These pathways were often linked to proliferation inhibition, drug-resistance modulation, EMT suppression, or apoptosis regulation. Autophagy and lysosomal/autophagic-flux regulation appeared in 5 studies (20.8%), indicating that autophagy-related responses were present but context-dependent, ranging from pro-apoptotic autophagy modulation to protective or incomplete autophagy.

Less frequent but mechanistically distinct categories included ROS/DNA-damage-related cytotoxicity in 4 studies (16.7%) and pyroptosis, EGFR/VEGFR-TKI signaling, Wnt/β-catenin/stemness signaling, and immune-mediated antitumor activity, each reported in 2 studies (8.3%). These lower-frequency pathways were not broadly represented across the dataset but provided important mechanistic specificity, particularly for inflammasome-mediated pyroptosis, β-catenin-associated stemness suppression, and immune-mediated cytotoxicity.

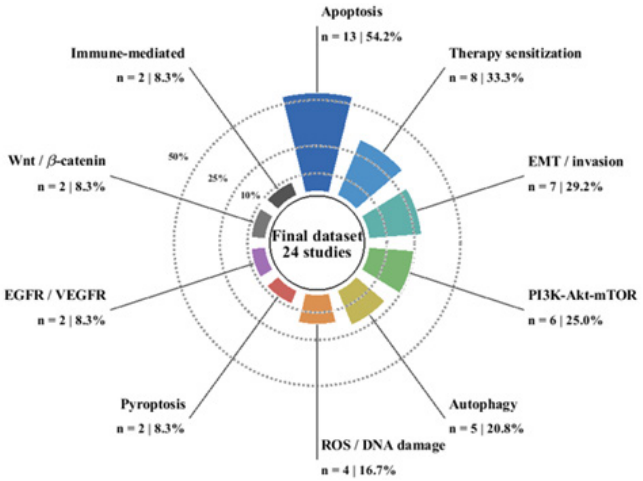

Figure 6: Radial mechanistic evidence map of active ingredients from Traditional Chinese Medicine in NSCLC.

5. Discussion

This meta-analysis synthesized evidence from 24 preclinical studies evaluating active ingredients from Traditional Chinese Medicine in NSCLC models. The final evidence base was dominated by in vitro cellular experiments, with 23 studies using conventional 2D NSCLC cell-line systems and one study incorporating patient-derived lung adenocarcinoma organoids. Although animal, xenograft, orthotopic, immune-competent, or PDOX components were present in a subset of studies, the overall body of evidence remains primarily experimental rather than clinical. This distribution is important for interpretation: the findings support biological plausibility and mechanistic activity, but they do not yet establish clinical efficacy in patients with NSCLC.

The most consistent biological effect across the included studies was a reduction in cell viability or proliferation. Direct IC50 or IC-range data were available in 13 studies, allowing comparison of potency across compounds, models, and treatment contexts. The lowest μM-scale IC50 values were observed for polyphyllin II in H1299 cells and α-hederin in A549 cells, whereas bufalin showed nanomolar activity in A549 and H460 cells and retained low-nanomolar potency across multiple NSCLC cell lines [12, 16, 21, 23]. Oridonin, honokiol, oxymatrine, chelerythrine chloride, patchouli alcohol, and ginsenoside Rd also showed measurable growth-inhibitory effects, although their potencies differed substantially across cell models, exposure durations, and assay contexts [2, 3, 5, 10, 19, 22]. This heterogeneity suggests that compound potency cannot be interpreted independently of cell-line background, treatment duration, and endpoint definition.

Apoptosis and regulated cell death signaling constituted the dominant mechanistic axis, observed in more than half of the included studies. Several compounds induced classical apoptotic responses through caspase activation, mitochondrial regulation, p53-associated signaling, or modulation of Bax/Bcl-2-related markers [1, 3-7, 11, 12, 16, 19, 22, 24]. The strongest directly reported apoptotic percentage responses included osthole plus embelin in A549 cells, patchouli alcohol-induced TUNEL positivity in both parental and vincristine-resistant A549 models, and ginsenoside Rd-associated apoptosis [4, 19, 22]. These findings indicate that apoptosis is a central mechanism by which multiple TCM-derived active ingredients exert antitumor effects in NSCLC models. However, direct quantitative comparability remains limited because of differences in apoptosis assays, doses, exposure times, and reporting formats across studies.

Beyond apoptosis, the included studies identified several additional regulated cell death and stress response mechanisms. Polyphyllin VI and sodium new houttuyfonate supported a pyroptosis-oriented mechanism involving inflammasome-related signaling, including the ROS/NF-κB/NLRP3/GSDMD axis and the TCONS-14036/miR-1228-5p/PRKCDBP pathway, respectively [13,18]. Autophagy-related mechanisms were more context-dependent. Honokiol and polyphyllin II linked autophagy modulation to growth inhibition or apoptosis, whereas α-hederin induced incomplete autophagic injury through impaired lysosomal acidification, and cycloastragenol activated apoptosis, along with protective autophagy, through the AMPK/ULK1/mTOR axis [3, 16, 23, 24]. These findings indicate that autophagy should not be interpreted uniformly as either cytotoxic or protective; rather, its functional role depends on the compound, pathway context, and experimental model.

A major finding of the synthesis was the importance of treatment sensitization. Several studies examined active ingredients as modulators of chemotherapy, targeted therapy, immunotherapy, or radiotherapy rather than as isolated cytotoxic agents. Oridonin showed synergistic interaction with docetaxel, with all reported combination-index values below 1.0 [2]. Emodin substantially reduced the IC50 of paclitaxel in A549 cells, supporting chemosensitization [7]. Tanshinone IIA reversed gefitinib resistance in HCC827/gefitinib and PC-9/gefitinib models, with marked reductions in gefitinib IC50 [9]. Bufalin increased radiosensitivity across A549, H1299, and HCC827 cells, with the strongest SERD0 observed in HCC827 cells [21]. In addition, andrographolide enhanced antitumor immunity in combination with anti-PD-1 treatment, and ginsenoside Rg3 improved cisplatin-response assessment in patient-derived organoid models [17, 20]. Together, these findings suggest that the most translationally relevant role of several TCM-derived compounds may be as sensitizers or resistance-modifying agents rather than only as monotherapies.

The mechanistic synthesis also highlighted recurrent survival, invasion, and resistance pathways. PI3K/Akt/mTOR or Akt-related signaling was implicated across multiple treatment contexts, including astragaloside IV, emodin/paclitaxel, tanshinone IIA/gefitinib, ellagic acid, polyphyllin II, and cycloastragenol [6, 7, 9, 11, 16, 24]. EGFR/VEGFR-related signaling was particularly relevant to oridonin and tanshinone IIA studies in the context of resistance or targeted therapy [2, 9]. EMT, migration, invasion, and metastasis-related outcomes were reported in studies involving oridonin, oxymatrine, astragaloside IV, chelerythrine chloride, bufalin plus radiation, ginsenoside Rd, and α-hederin [2, 5, 6, 10, 21-23]. Wnt/β-catenin and stemness-related signaling were less frequently reported but were mechanistically important in astragaloside IV and chelerythrine chloride studies [6, 10]. These results show that the antitumor effects extended beyond cytotoxicity to include progression-related phenotypes and resistance-associated signaling.

Advanced model evidence strengthened the biological relevance of selected findings but remained unevenly distributed. Xenograft or animal-based validation was reported for oridonin, emodin plus paclitaxel, tanshinone IIA plus gefitinib, polyphyllin VI, tanshinone IIA with NK-cell transfer, andrographolide, sodium new houttuyfonate, and cycloastragenol [2, 7, 9, 13, 15, 17, 18, 24]. These models supported in vivo antitumor activity, chemosensitization, resistance reversal, pyroptosis-related tumor suppression, and immune-mediated effects. The ginsenoside Rg3 study was notable because it used patient-derived lung adeno-

carcinoma organoids and PDOX characterization, providing a platform closer to patient-level heterogeneity than conventional cell lines [20]. However, because only one included study used PDOs, the evidence for patient-derived translational modeling remains preliminary.

Several limitations should be considered. First, the included evidence is preclinical and heterogeneous, with substantial variation in cell lines, compound concentrations, treatment durations, assay types, and outcome definitions. Second, although IC50 values were available in 13 studies, many key endpoints were reported only as pathway changes, representative images, or non-uniform percentage outcomes, limiting formal quantitative pooling across all studies. Third, only a minority of studies used advanced animal or organoid models, and most relied on 2D cell line systems. Fourth, sensitization studies combined different therapeutic contexts, including chemotherapy, EGFR-TKI resistance, radiotherapy, NK-cell activity, anti-PD-1 therapy, and organoid-based cisplatin response, which should be interpreted as biologically distinct rather than directly interchangeable [2, 7, 9, 15, 17, 20, 21].

6. Conclusion

This meta-analysis indicates that active ingredients from Traditional Chinese Medicine exert multifaceted antitumor effects in NSCLC preclinical models. The strongest evidence supports cytotoxicity, inhibition of proliferation, induction of apoptosis, and modulation of key survival and resistance-related pathways. Several compounds also enhanced chemotherapy, EGFR-TKI response, radiotherapy, immune-mediated cytotoxicity, or cisplatin sensitivity in organoid-based models, suggesting a potential role as treatment-sensitizing agents. However, the evidence remains predominantly preclinical and heterogeneous, with limited patient-derived and in vivo validation. Future studies should prioritize standardized quantitative reporting, mechanistically validated combination strategies, and translational testing in patient-derived organoids, PDOX models, and clinically relevant NSCLC systems.

7. Funding

This study was supported by the National Natural Science Foundation of China (Grant No. 82174030), the Henan Province Science and Technology Research and Development (Grant Nos. 252102311246, 242102310512, 242102110202), and the Xinyang Agriculture and Forestry University Youth Fund Project (No. QN2023028). The funders had no role in study design, data collection and analysis, decision to publish, or preparation of the manuscript.

References

1. Li X. Triptolide reduces proliferation and enhances apoptosis of human non-small cell lung cancer cells through PTEN by targeting miR-21. Molecular medicine reports. 2016; 13(3): 2763-2768.
2. Xiao X. Oridonin inhibits gefitinib-resistant lung cancer cells by suppressing EGFR/ERK/MMP-12 and CIP2A/Akt signaling pathways. International Journal of Oncology. 2016; 48(6): 2608-2618.
3. Luo LX. Honokiol induces apoptosis, G1 arrest, and autophagy in KRAS mutant lung cancer cells. Frontiers in pharmacology. 2017; 199.
4. Xu XM. Osthole induces lung cancer cell apoptosis through inhibition of inhibitor of apoptosis family proteins. Oncology Letters. 2016; 12(5): 3779-3784.
5. Izdebska M. The cytotoxic effect of oxymatrine on basic cellular processes of A549 non-small lung cancer cells. Acta Histochemica. 2019; 121(6): 724-731.
6. Jia L. Astragaloside IV inhibits the progression of non-small cell lung cancer through the Akt/GSK-3β/β-catenin pathway. Oncology research. 2019; 27(4): 503.
7. Chen SZ, Zhang, J Zhang. Emodin enhances antitumor effect of paclitaxel on human non-small-cell lung cancer cells in vitro and in vivo. Drug design, development and therapy. 2019; 1145-1153.
8. Zhang J. Cytological effects of honokiol treatment and its potential mechanism of action in non-small cell lung cancer. Biomedicine & Pharmacotherapy. 2019; 117: 109058.
9. Wang R. Tanshinone IIA reverses gefitinib-resistance in human non-small-cell lung cancer via regulation of VEGFR/Akt pathway. OncoTargets and therapy. 2019; 9355-9365.
10. Heng WS, SC Cheah. Chelerythrine chloride downregulates β-catenin and inhibits stem cell properties of non-small cell lung carcinoma. Molecules. 2020; 25(1): 224.
11. Liu, Q. Ellagic acid promotes A549 cell apoptosis via regulating the phosphoinositide 3-kinase/protein kinase B pathway. Experimental and therapeutic medicine. 2018; 16(1): 347-352.
12. Kim NY. Bufalin down-regulates Axl expression to inhibit cell proliferation and induce apoptosis in non-small-cell lung cancer cells. Bioscience Reports. 2020; 40(4): BSR20193959.
13. Teng JF. Polyphyllin VI induces caspase-1-mediated pyroptosis via the induction of ROS/NF-κB/NLRP3/GSDMD signal axis in non-small cell lung cancer. Cancers. 2020; 12(1): 193.
14. Li M. Emodin regulates cell cycle of non-small lung cancer (NSCLC) cells through hyaluronan synthase 2 (HA2)-HA-CD44/receptor for hyaluronic acid-mediated motility (RHAMM) interaction-dependent signaling pathway. Cancer Cell International. 2021; 21(1): 19.
15. Sun Y. Tanshinone IIA enhances susceptibility of non-small cell lung cancer cells to NK cell-mediated lysis by up-regulating ULBP1 and DR5. Journal of Leukocyte Biology. 2021; 110(2): 315-325.
16. Jiao Y. Polyphyllin II induced apoptosis of NSCLC cells by inhibiting autophagy through the mTOR pathway. Pharmaceutical biology, 2022. 60(1): p. 1781-1789.
17. Wang XR. Andrographolide suppresses non-small-cell lung cancer progression through induction of autophagy and antitumor immune response. Pharmacological Research. 2022; 179: 106198.
18. Jiang R. The sodium new houttuyfonate suppresses NSCLC via activating pyroptosis through TCONS-14036/miR-1228-5p/PRKCDBP pathway. Cell Proliferation. 2023; 56(7): e13402.
19. Liang CY. Patchouli alcohol induces G0/G1 cell cycle arrest and apoptosis in vincristine-resistant non-small cell lung cancer through ROS-mediated DNA damage. Thoracic Cancer. 2023; 14(21): 2007-2017.

20. Liu M. Ginsenoside Rg3 promotes chemosensitivity in lung adenocarcinoma organoids via apoptotic pathways. Frontiers in Pharmacology. 2026; 17: 1791170.

21. Wang Z. Bufalin inhibits epithelial-mesenchymal transition and increases radiosensitivity of non-small cell lung cancer via inhibition of the Src signaling. Journal of Thoracic Disease. 2023; 15(1): 123.

22. Wan X. Ginsenoside Rd reduces cell proliferation of non-small cell lung cancer cells by p53-mitochondrial apoptotic pathway. Heliyon. 2024; 10(11).

23. Jin F. Alpha-Hederin induces incomplete autophagic injury in non-small cell lung cancer by interfering with the lysosomal acidification. Scientific reports. 2024; 14(1): 13258.

24. Zhu LH. Cycloastragenol induces apoptosis and protective autophagy through AMPK/ULK1/mTOR axis in human non-small cell lung cancer cell lines. Journal of integrative medicine. 2024; 22(4): 503-514.